



Impact risk assessment and planetary defense mission planning for asteroid 2015 PDC



George Vardaxis^{a,*}, Peter Sherman^b, Bong Wie^a

^a Asteroid Deflection Research Center, Department of Aerospace Engineering, Iowa State University, 2348 Howe Hall, Ames, IA 50011-2271, USA

^b Department of Statistics, Department of Aerospace Engineering, Iowa State University, 2339 Howe Hall, Ames, IA 50011-2271, USA

ARTICLE INFO

Article history:

Received 13 June 2015

Received in revised form

4 January 2016

Accepted 9 February 2016

Available online 16 February 2016

Keywords:

Impact risk

Impact probability

Asteroid 2015 PDC

Planetary defense

Mission design

Keyholes

ABSTRACT

In this paper, an integrated utilization of analytic keyhole theory, B-plane mapping, and planetary encounter geometry, augmented by direct numerical simulation, is shown to be useful in determining the impact risk of an asteroid with the Earth on a given encounter, as well on potential future encounters via keyhole passages. The accurate estimation of the impact probability of hazardous asteroids is extremely important for planetary defense mission planning. Asteroids in Earth resonant orbits are particularly troublesome because of the continuous threat they pose in the future. Based on the trajectories of the asteroid and the Earth, feasible mission trajectories can be found to mitigate the impact threat of hazardous asteroids. In order to try to ensure mission success, trajectories are judged based on initial and final mission design parameters that would make the mission easier to complete. Given the potential of a short-warning time scenario, a disruption mission considered in this paper occurs approximately one year prior to the anticipated impact date. Expanding upon the established theory, a computational method is developed to estimate the impact probability of the hazardous asteroid, in order to assess the likelihood of an event, and then investigate the fragmentation of the asteroid due to a disruption mission and analyze its effects on the current and future encounters of the fragments with Earth. A fictional asteroid, designated as 2015 PDC – created as an example asteroid risk exercise for the 2015 Planetary Defence Conference, is used as a reference target asteroid to demonstrate the effectiveness and applicability of computational tools being developed for impact risk assessment and planetary defense mission planning for a hazardous asteroid or comet.

© 2016 IAA. Published by Elsevier Ltd. All rights reserved.

1. Introduction

There is a very real and ever-present threat that Earth faces every day from asteroids. Most of the impacts are from objects that are too small to cause any damage on the surface due to the fact that they break up in the atmosphere.

However, there are the rare occurrences where an object does make landfall and causes some serious damage. With the increased efforts and capabilities of identifying potentially hazardous near-Earth asteroids (NEAs), the pool of unknown objects is decreasing and they are becoming classified as known objects with zero risk. However, there is a non-zero potential for one of those unknown bodies to pose a serious threat to the Earth. Fortunately, the human race is in a unique position to do something about those threats, to either mitigate or eliminate them.

* Corresponding author.

E-mail addresses: gwardaxis@gmail.com (G. Vardaxis), shermanp@iastate.edu (P. Sherman), bongwie@iastate.edu (B. Wie).

Dealing with the threat of any near-Earth object (NEO) has three main steps: detection/tracking, characterization, and mitigation. NASA, as well as other organizations, has put a lot of effort into the detection/tracking of all NEOs, both threatening and non-threatening. At the Asteroid Deflection Research Center (ADRC) of Iowa State University, there has been extensive research on mitigation methods regarding NEOs with short warning times (< 10 years) by studying potential mission designs to disrupt hazardous asteroids. This paper is concerned with asteroid 2015 PDC [1], the disruption mission trajectory design for a Hypervelocity Asteroid Intercept Vehicle (HAIV) to the target body [2,3], as well as the methodology used to assess the impact risk of an asteroid and its fragments on their current and future encounters with the Earth.

A hypothetical impact scenario of fictional asteroid 2015 PDC is considered in this paper. As described in [1], the scenario begins as follows: the asteroid is discovered on April 13, 2015, the first day of the conference, it is assigned the designation “2015 PDC” by the Minor Planet Center, and classified as a Potentially Hazardous Asteroid (PHA) based on its orbit. The asteroid’s orbital elements are known fairly accurately even in the first few days: semi-major axis (a) is 1.77 AU, the orbital eccentricity (e) is 0.49, its perihelion distance (q) is 0.90 AU and aphelion distance (Q) is 2.65 AU, the orbital period (TP) is 864 days (2.37 years), and the orbital inclination (i) is a fairly small 5.35° . Despite the seemingly accurate values of the orbital elements, very little is known about the object’s physical properties due to uncertainties in both the albedo and absolute magnitude values. The asteroid’s absolute magnitude (H) is estimated to be about $H=21.3 \pm 0.4$, which puts the asteroid’s size at roughly 100–500 m. The JPL Sentry system and University of Pisa’s CLOMON system both identify many potential impacts for this object at several future dates. The most likely potential impact date is September 3, 2022, but the impact probability for that date is still low in the first week after the asteroid is discovered. Nevertheless, as the object is tracked over the next few weeks, the impact probability for 2022 starts to climb, reaching 0.2% a month after discovery. As the asteroid continues to be observed and tracked, the chance of impact just keeps rising. The first part of the scenario ends in mid-June 2015, when the probability of Earth impact in 2022 has reached 1% and continues to rise. It is at this point that this paper begins its analysis and proceeds from, despite the fact that the rest of the scenario was to be played out at the conference.

This paper is essentially broken into two parts: the first being a description of the tools and methods used to conduct the analyses and the second being the results regarding mission design, fragmentation, and impact probability analyses.

The first part of the paper is further broken down into four sections: Asteroid Mission Design Software Tool (AMiDST), Impact Risk Assessment of Asteroid 2015 PDC, Impact and Keyhole Passage Risk Assessment, and Analytic Keyhole Theory. In Section 2, an in-house mission design tool, named AMiDST [4], will be briefly described. While it does not have the high-fidelity trajectory optimization as some of the existing trajectory and mission optimization

tools (such as Mystic, MALTO, Copernicus, SNAP, OTIS, and GMAT), it focuses instead on the launch and terminal phases of the NEO mitigation mission design. AMiDST looks into several launch vehicle and spacecraft configurations based upon several evaluation criteria such as launch vehicle mass capacity and mission ΔV requirements, as well as relative approach velocity and approach angle. In addition to these features, it also provides an estimated total mission cost, used only as a final determination factor between mission configurations. Section 3 discusses the propagation models and the construction of the orbital uncertainties used in the modeling of the impact risk posed by an asteroid. A high-fidelity gravitational model is used to propagate the asteroid body, along with the field of virtual asteroids constructed from the orbital uncertainties, forward in time to see if and/or when it would come in close proximity to a planet, particularly Earth, possibly resulting in a change of the asteroid’s orbit, in either size (semi-major axis), shape (eccentricity) and/or orientation (inclination, argument of periape, and longitude of the ascending node). Section 4 discusses the theory associated with calculating the impact risk posed by an asteroid and the likelihood of an asteroid passing through a gravitational keyhole. And Section 5 discusses analytic keyhole theory, in terms of target B-planes, resonant return orbits, and gravitational keyholes. Techniques such as a high-precision gravitational simulator, encounter geometry, B-plane mapping, and gravitational keyholes are used in this paper to quantitatively evaluate the orbital characteristics of an asteroid and its associated impact risk. From the encounter geometry, the post-encounter heliocentric orbit of the asteroid could be in resonance with the planet resulting in another encounter, or potentially an impact. Taking advantage of an asteroid’s encounter B-plane (the two-dimensional plane perpendicular to asteroid’s velocity vector at its closest approach to the encountering planet) and analytic keyhole theory (the theory that estimates the existence of Earth-asteroid resonance orbits, as well as the size and location of Earth in the future – on the current encounter B-planes), an estimate of the current and future impact probability of the asteroid can be obtained.

The second part of the paper presents the results of the analyses conducted regarding asteroid 2015 PDC. Section 6 of the paper discusses several mission design options for asteroid 2015 PDC, including the inability to conduct a feasible rendezvous mission and various types of disruption missions. The disruption mission analyses are partitioned into combinations of short (< 90 days) and long (> 200 days) duration and dispersion missions. Finally, Section 7 discusses the fragmentation analysis of asteroid 2015 PDC. Utilizing the orbital uncertainty modeling described in Section 3, a virtual debris cloud from an asteroid propagation is created and propagated through Earth encounter to understand the potential variability in the cloud’s encounter. Once there is an understanding of the cloud’s encounter with the Earth, a single asteroid fragment is selected, based on its Earth encounter, and an uncertainty cloud is constructed around that fragment and is propagated through the Earth encounter and analyzed

to see the likelihood of that fragment passing through a keyhole or impacting the planet on the current encounter.

2. Asteroid Mission Design Software Tool (AMiDST)

An in-house mission design tool, called AMiDST, is used to conduct the mission and trajectory design for NEO mitigation missions. Fig. 1 shows a flowchart of the various mission design components and general operations of the AMiDST program, including spacecraft selection, launch vehicle selection, and mission cost estimation.

2.1. AMiDST components

In order to run the AMiDST program, the user must input the type of spacecraft that will be used to conduct

the mission. The user has two possible spacecraft configurations, a single-body kinetic impactor and a two-body HAIV spacecraft. The desire to use a spacecraft concept like the HAIV comes from the fact that most direct intercept missions with a short warning time (< 10 years) will result in relative arrival velocities of 10–30 km/s. The current nuclear subsurface penetrator technology limits the impact velocity to less than about 300 m/s, due to the fact that higher impact speeds prematurely destroy the fusing mechanisms of the nuclear explosive devices (NEDs) [5,6]. The HAIV concept was developed in order to overcome these technological limitations [2].

Mission cost estimation to design and fabricate the missions is an important task necessary for early assessment of mission viability and feasibility. The final total cost of each mission is given as a combination of the cost for the launch vehicle, the spacecraft, and estimated mission

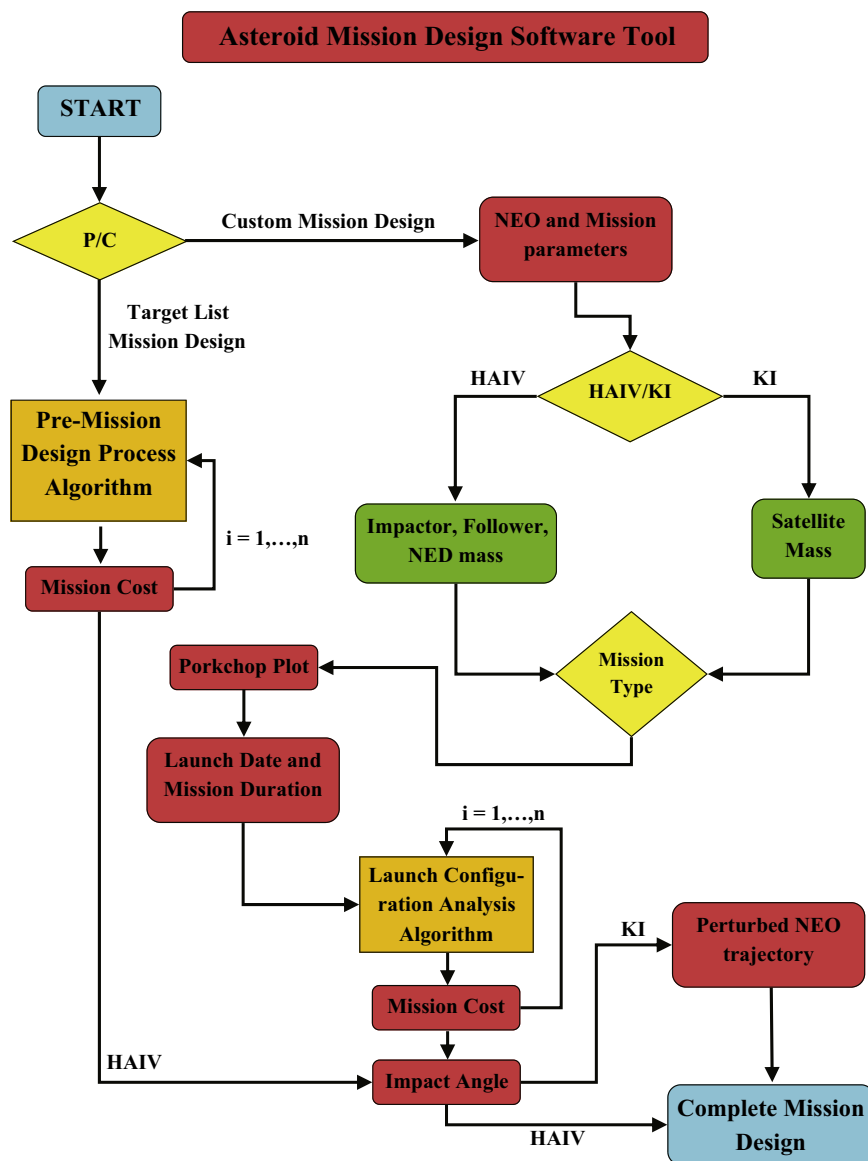


Fig. 1. Flowchart illustration of the AMiDST.

operations. A cost estimation algorithm was developed to determine the costs associated with constructing the spacecraft, based on a number of previous spacecraft missions with similar goals and parameters. Spacecraft such as Deep Impact, Stardust, and Dawn were researched to find the cost of developing such spacecraft and a linear polynomial fit was applied to the data to come up with an analytic formula relating spacecraft mass and cost. As a comparison, the initial mission cost estimates were run through NASA's Advanced Mission Cost Model (AMCM) [7], to get a rough order of magnitude approximation. The estimates from the AMCM came out to be rather rough when it comes to estimating the cost of the constructing the HAIV spacecraft, mostly due to the fact that the HAIV designs do not exactly fit into a single mission category from the available choices. However, the estimates did verify that the estimates are in the appropriate cost range.

The entire design space of mission durations and launch dates, as specified by the user, is analyzed using a customizable cost function according to user-defined mission parameters. The potential design variables are

$$\mathbf{X} = [JD, \Delta V, C3, dispersion, duration, v_{arr}, \alpha_{arr}, \alpha_{LOS}, \alpha_{Sun}] \quad (1)$$

where JD represents the Julian date at mission departure, ΔV is the total mission change in velocity required, $C3$ is the associated mission hyperbolic excess energy at departure from Earth's sphere of influence, $dispersion$ is the amount of time between the impact of the spacecraft with the asteroid and the expected asteroid impact date with the Earth, $duration$ is the transfer time of the spacecraft from its Earth launch to the encounter with the target asteroid, v_{arr} is the relative arrival velocity between the asteroid and the spacecraft, α_{arr} is the relative arrival angle between the asteroid and spacecraft at intercept, α_{LOS} is the line-of-sight angle between Earth and the asteroid at the time of intercept, and α_{Sun} is the approach angle of the spacecraft to the asteroid with respect to the Sun. The cost function is constructed in the following manner

$$C(\mathbf{X}) = f(\mathbf{X}) + g(\mathbf{X}) \quad (2)$$

where $f(\mathbf{X})$ is a constant cost attributed to every mission trajectory and $g(\mathbf{X})$ is a variable cost that is dependent on the state variables used within the trajectory optimization [8]. The components of the overall cost function $f(\mathbf{X})$ and $g(\mathbf{X})$ take the form

$$f(\mathbf{X}) = \Delta V + \sqrt{C3} \quad (3)$$

and

$$g(\mathbf{X}) = g(JD) + g(dispersion) + g(duration) + g(v_{arr}) + g(\alpha_{arr}) + g(\alpha_{LOS}) + g(\alpha_{Sun}) \quad (4)$$

The component cost functions are defined based on the user defined upper and lower bounds for the state variables used in the cost function evaluation of the mission design space. The resulting cost function score will vary between different mission possibilities due to the difference in state variable values, but the way in which the score is calculated is based on the $f(\mathbf{X})$ and $g(\mathbf{X})$ functions listed above.

3. Impact Risk Assessment of Asteroid 2015 PDC

Before any work can be done in relation to rendezvous or disruption mission designs, a certain degree of understanding must be reached in reference to the asteroid's imposed threat to the Earth.

3.1. Propagation models

The dynamics that govern the motion of an asteroid in space are highly dependent on the model that is used to predict the body's orbital trajectory. Within the framework of the work described in this paper, two dynamical models are used: the so-called Standard Dynamical Model (SDM) for simulating the orbital motion of the asteroid body and a three-body system that incorporates on the effects of the Earth, Moon, and J_2 perturbation for when the asteroid body has passed within the sphere of influence (SOI) of the Earth. The orbit propagation uses a variable stepsize Runge–Kutta Fehlberg (RKF) 7(8) method that takes into account the effects of the Sun, all eight planets, Pluto, the three largest main belt asteroids (Ceres, Pallas, Vesta), Earth's Moon, as well as the option to include solar radiation pressure and relativistic effects. Given the short amount of time that the asteroid spends within the Earth SOI, the added perturbations from the Sun and other planets do not amount to enough to warrant their inclusion within the dynamical model used for that system.

The Standard Dynamical Model takes the form [9]

$$\frac{d^2 \vec{r}}{dt^2} = -\frac{\mu}{r^3} \vec{r} + \sum_{k=1}^n \mu_k \left(\frac{\vec{r}_k - \vec{r}}{|\vec{r}_k - \vec{r}|^3} - \frac{\vec{r}_k}{r_k^3} \right) + \vec{f} \quad (5)$$

where \vec{r} is the heliocentric position of the propagating body, $\mu = GM$ is the gravitational parameter of the Sun, n is the number of perturbing bodies, μ_k and \vec{r}_k are the gravitational parameter and heliocentric position vector of perturbing body k , respectively, and \vec{f} represents other non-conservative orbital perturbation acceleration [9]. The equation itself is broken into three separate, distinct terms – the first term is the gravitational effect of the Sun on the propagating body, the second term is the combined third body effects of other planetary bodies like planets, moons, and other asteroids, and finally the third term represents non-conservative effects. The three most well-known non-conservative orbital perturbations are solar radiation pressure (SRP), relativistic effects, and the Yarkovsky effect, the former two being the most prevalent effects. Solar radiation pressure provides a radial outward force on the asteroid body from the interaction of the Sun's photons impacting the asteroid surface. The SRP model is given by

$$\vec{a}_{SRP} = (K)(C_R) \left(\frac{A_R}{M} \right) \left(\frac{L_S}{4\pi cr^2} \right) \vec{r} \quad (6)$$

where \vec{a}_{SRP} is the solar radiation pressure acceleration vector, C_R is the coefficient for solar radiation ($\approx -4.51e-6 \text{ N/m}^2$), A_R is the cross-sectional area of the body presented to the Sun, M is the mass of the asteroid, K is the fraction of the solar disk visible at the asteroid's location, L_S is the luminosity of the Sun ($3.846e26 \text{ W}$), c is the speed

of light, and \vec{r} and r are the distance vector and magnitude of the asteroid from the Sun, respectively [10]. The relativistic effects of the body are included because for many objects, especially those with small semi-major axes and large eccentricities, those effects introduce a non-negligible radial acceleration toward the Sun. One form of the relativistic effect is represented by

$$\vec{a}_R = \frac{k^2}{c^2 r^3} \left[\frac{4k^2 \vec{r}}{r} - (\dot{\vec{r}} \cdot \dot{\vec{r}}) \vec{r} + 4(\vec{r} \cdot \dot{\vec{r}}) \dot{\vec{r}} \right] \quad (7)$$

where \vec{a}_R is the acceleration vector due to relativistic effects, k is the Gaussian constant, c is the speed of light, \vec{r} is the position vector of the asteroid, and $\dot{\vec{r}}$ is the velocity vector of the asteroid [11].

Within the Earth's SOI a similar dynamical model is used to that shown in Eq. (5), where the main gravitating body is the Earth instead of the Sun, the Moon is treated as the only perturbing body, and \vec{f} is the J_2 perturbation. In the Cartesian frame that the propagation would be done in, the J_2 perturbation takes the following form

$$\ddot{x} = -\frac{\mu x}{r^3} - 3\kappa \left(\frac{x}{r^5} \right) \left(1 - \frac{5z^2}{r^2} \right) \quad (8)$$

$$\ddot{y} = -\frac{\mu y}{r^3} - 3\kappa \left(\frac{y}{r^5} \right) \left(1 - \frac{5z^2}{r^2} \right) \quad (9)$$

$$\ddot{z} = -\frac{\mu z}{r^3} - 3\kappa \left(\frac{z}{r^5} \right) \left(3 - \frac{5z^2}{r^2} \right) \quad (10)$$

where $\kappa = J_2 \mu R_\oplus^2 / 2$, $r = \sqrt{x^2 + y^2 + z^2}$, μ is the Earth's gravitational parameter, J_2 is the value of the second zonal harmonic, and R_\oplus is the mean Earth's equatorial radius. The coordinate system is inertially fixed with the (x, y) plane corresponding to the Earth's equatorial plane [12].

For relatively short-term simulations (less than 10–20 years), the inclusion of non-conservative effects in the propagation model will not greatly effect the position and velocity of the propagated body over time due to their small added perturbations. Taking into account the non-gravitational perturbations in the free-space and flyby propagations, the error within the systems will increase, but their inclusions would be needed in order to maintain consistency when the body's states are compared with the planetary ephemeris. To ensure the more accurate computation of the asteroid state vector, and the calculation of asteroid impact probabilities and gravitational keyholes, a more complete dynamical model for either the free-space or flyby propagation would need to be used, therefore leading to more effective mission designs.

3.2. Impact probability estimation

To arrive at probability distributional information at an encounter location with Earth, given uncertainties associated with an initial condition years and millions of kilometers from the encounter, is not possible due to the nonlinearities associated with Eqs. (5), (8)–(10). Nonetheless, mitigation strategies considered in this work would need to be implemented at least a year prior to the encounter, to give plenty of time for the asteroid fragments to disperse in the case of a successful disruption

mission. Hence, simulations are essential in order to arrive at a probabilistic description of the uncertainty associated with an expected encounter.

The estimated impact date of asteroid 2015 PDC with Earth is September 3, 2022, based on the nominal trajectory given by JPL. In this work the initial condition date is chosen to be September 2, 2021. The initial condition uncertainty is associated with the 6-dimensional random variable that includes the position and velocity components associated with Eqs. (5), (8)–(10). One source of the uncertainty is related to the resolution of sensors used to estimate the initial state, however this work does not include a sensor sensitivity analysis needed to produce the stated orbital uncertainties. In this work we will assume that the three position uncertainty components are mutually independent and identically distributed (iid) with a normal probability density function (pdf) having zero mean and standard deviation to 50 m. Similarly, we assume that the velocity uncertainty components are iid and normally distributed with zero mean and standard deviation equal to 10 m/s. Finally, we assume that the position and velocity uncertainties are also mutually independent.

Clearly, the above assumptions are ad hoc in nature. In statistical jargon the resulting distribution is known as an ignorance prior pdf. Were the goal of this work to carry out an exhaustive probabilistic analysis, it would be necessary to investigate not only the details of the sensors being used, but also the dynamics associated with a given nominal initial condition. Such an investigation can be carried out in future work. The goal of this work is, in part, to lay the foundation for such an investigation by gaining an appreciation for the behavior of the encounter uncertainty under the simplest conditions.

In addition to simulating the nominal asteroid state through to the encounter date under no initial condition uncertainty, 2000 simulations were run via random sampling of the initial condition pdf described above. The scatter plot of the close approach encounter coordinates is shown in Fig. 2. Even though the components of the initial condition (X, Y, Z) coordinates were iid, we see that the close approach encounter coordinates are highly correlated. While such correlation may be generally expected due to the dynamics, the simulations provided quantified support for this expectation. It should be mentioned that Fig. 2 includes only 1304 of the total 2001 simulations.

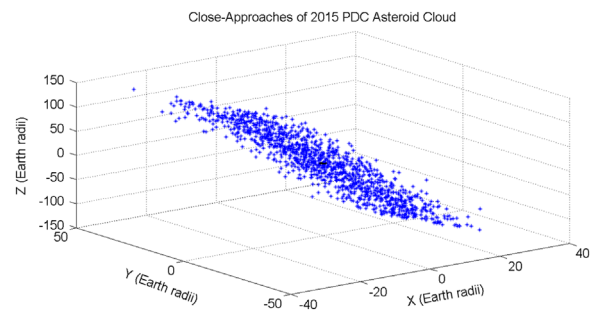


Fig. 2. Representation of the virtual asteroid cloud close approaches with initial uncertainties of 50 m and 10 m/s in each coordinate direction, with respect to the Earth's surface.

The remaining 697 simulations did not achieve a close encounter with the Earth. While not visually obvious, only two simulations resulted in an Earth impact, one of which was the simulation representing the unaltered asteroid state. The results from this batch of simulations show a very small impact probability (0.153%) for the encountering asteroid body, which was estimated to be around 1% at the time of its discovery on April 13, 2015. The number of simulations used in the previous analysis was too small to arrive at a reliable estimate of the impact probability. However, the use of such a small number of simulations is helpful in order to gain an understanding of the appropriate position and velocity errors for the asteroid state uncertainty to be comparable to similar asteroids.

A standard deviation error of position and velocity provides a good measure of the position and velocity variations. But, the best way to understand how initial conditions vary, not only individually but with each other, as compared to other asteroids is to consider a covariance matrix. Table 1 provides the covariance matrix of the orbital element initial conditions discussed previously. In Table 1, a denotes the semi-major axis (in units of AU), e the eccentricity, i the inclination, Ω the longitude of the ascending node, ω the argument of periaapse, and θ_0 the true anomaly angle at epoch – all the angles are in units of degrees. It can be seen that while there is fairly little variation in semi-major axis and eccentricity, the inclination and all the angles that define the orbit's orientation and the position of the body in the orbit have rather large variance and covariance values. In comparison to other near-Earth asteroids, the covariance matrix for 2015 PDC in this scenario is too large to be realistic for such an asteroid.

If we narrow the velocity component variations from 10 m/s to 1 m/s, with the same position component variations and epoch, it is found that all 2001 of the virtual asteroids cross the Earth's SOI and have an encounter with the Earth. The various depths of encounter for the virtual asteroid cloud can be seen in Fig. 3. The impact probability for 2015 PDC, given these position and velocity uncertainties, comes to be about 3.05%. Looking again at the initial orbital element covariance matrix for this asteroid cloud it can be seen that the values in the covariance matrix have all decreased by about two orders of magnitude. This implies that changing the variation in the velocity components by an order of magnitude causes a change in the orbital element covariance matrix as a whole. While all the virtual asteroids have an encounter with Earth and the impact probability has gone up drastically, the covariance is still larger than most

near-Earth asteroids that have had several observations by Earth stations or satellites.

If 25 random asteroids (near-Earth asteroids included) are chosen and their covariance matrices are averaged, the corresponding position and velocity variations for asteroid 2015 PDC can be found so that a more accurate impact probability can be found at the given epoch. The asteroids used to compute an average asteroid covariance matrix to compare to that of asteroid 2015 PDC were asteroids with semi-major axes that were between 1 and 2 AU. Some of the notable asteroids that were selected to be a part of the sample were Apophis, Bennu, and 2011 AG5, the rest of the 25 asteroids were selected randomly using the previously mentioned semi-major axis criterion. The average orbital element covariance matrix of the 25 sample asteroids is shown in Table 3 where t_p is the time of periaapse given as a Julian Date and q is the perihelion distance in AU. Comparing a few of the values in Table 3 with those in Table 2, it can be seen that while the inclination and eccentricity variances are comparable, the variances of the longitude of the ascending node and argument of periaapse are orders of magnitude different.

As a final check of the impact risk of asteroid 2015 PDC, another 2,001 virtual asteroid simulation was run using

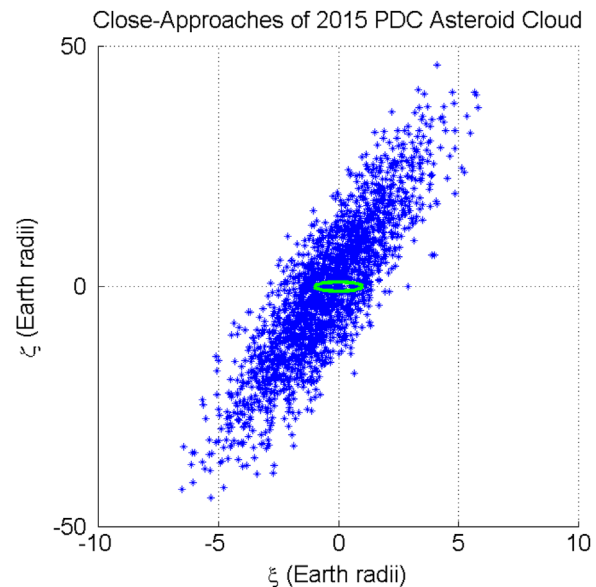


Fig. 3. Representation of the virtual asteroid cloud close approaches with initial uncertainties of 50 m and 1 m/s in each coordinate direction, with respect to the Earth's surface.

Table 1

Orbital element covariance matrix for 2001 virtual asteroid simulation based on normally distributed initial conditions with 50-m σ position uncertainty and 10-m/s σ velocity uncertainty.

	a	e	i	Ω	ω	θ_0
a	1.018e−06	−6.574e−07	1.436e−06	−8.602e−06	−4.205e−05	5.062e−05
e	−6.574e−07	5.111e−07	−9.148e−07	5.498e−06	1.791e−05	−2.339e−05
i	1.436e−06	−9.148e−07	0.00127	−0.00769	0.00759	7.266e−05
Ω	−8.602e−06	5.498e−06	−0.00769	0.0465	−0.0459	−0.000433
ω	−4.205e−05	1.791e−05	0.00759	−0.0459	0.0487	−0.00308
θ_0	5.062e−05	−2.339e−05	7.266e−05	−0.000433	−0.00308	0.00351

Table 2

Orbital element covariance matrix for 2001 virtual asteroid simulation based on normally distributed initial conditions with 50-m σ position uncertainty and 1-m/s σ velocity uncertainty.

	a	e	i	Ω	ω	θ_0
a	1.0183e-08	-6.574e-09	1.434e-08	-8.662e-08	-4.198e-07	5.061e-07
e	-6.574e-09	5.111e-09	-9.146e-09	5.525e-08	1.788e-07	-2.338e-07
i	1.434e-08	-9.146e-09	1.273e-05	-7.696e-05	7.590e-05	7.248e-07
Ω	-8.662e-08	5.525e-08	-7.696e-05	0.000465	-0.000459	-4.376e-06
ω	-4.198e-07	1.788e-07	7.590e-05	-0.000459	0.000488	-3.073e-05
θ_0	5.061e-07	-2.338e-07	7.248e-07	-4.376e-06	-3.073e-05	3.509e-05

Table 3

Average orbital element covariance matrix for 25 randomly selected near-Earth asteroids with similar semi-major axis lengths to that of asteroid 2015 PDC.

	e	q	t_p	Ω	ω	i
e	3.240e-08	-4.014e-09	4.279e-07	5.105e-08	8.903e-09	9.819e-07
q	-4.014e-09	2.195e-09	-1.457e-07	1.788e-08	4.620e-08	-7.914e-08
t_p	4.279e-07	-1.457e-07	6.674e-05	-1.267e-06	3.396e-05	1.586e-05
Ω	5.105e-08	1.788e-08	-1.267e-06	6.571e-07	-5.703e-07	1.399e-06
ω	8.903e-09	4.620e-08	3.396e-05	-5.703e-07	3.044e-05	9.181e-06
i	9.819e-07	-7.914e-08	1.586e-05	1.399e-06	9.181e-06	3.503e-05

Table 4

Orbital element covariance matrix for 2001 virtual asteroid simulation based on normally distributed initial conditions with 1-m σ position uncertainty and 5-cm/s σ velocity uncertainty.

	a	e	i	Ω	ω	θ_0
a	2.546e-11	-1.643e-11	3.585e-11	-2.167e-10	-1.049e-09	1.265e-09
e	-1.643e-11	1.278e-11	-2.286e-11	1.382e-10	4.470e-10	-5.846e-10
i	3.585e-11	-2.286e-11	3.183e-08	-1.924e-07	1.897e-07	1.8116e-09
Ω	-2.167e-10	1.382e-10	-1.924e-07	1.163e-06	-1.147e-06	-1.095e-08
ω	-1.049e-09	4.470e-10	1.897e-07	-1.147e-06	1.219e-06	-7.681e-08
θ_0	1.265e-09	-5.846e-10	1.812e-09	-1.095e-08	-7.681e-08	8.771e-08

the same epoch, but with position and velocity uncertainties of one meter and five centimeters per second, respectively, in all three coordinate directions. Such small uncertainties brings the initial orbital element covariance matrix of 2015 PDC, much closer to that of the average asteroid for certain parameters and others are shown to be much smaller than their average asteroid counterpart, as shown in Table 4. The smaller orbital element variances that come from such small state vector uncertainties imply that the orbit is more well-defined at this late stage in the asteroid's trajectory, which would make sense given that it is a year from potentially impacting the planet. In fact, in this scenario asteroid 2015 PDC has about a 57% chance of impacting the Earth. If the impact probability for the asteroid is this high at the given point in time, it is more likely that the probability of an impact will increase as more observations are made as the encounter date draws closer, assuming that the asteroid remains along its mean orbital trajectory.

Several mitigation strategies exist for dealing with hazardous near-Earth asteroids. Research studies conducted by NASA and the National Research Council (NRC) suggest that certain strategies are preferred to others based on the available warning time and the asteroid diameter [13]. Based on Fig. 4 it is suggested that any asteroid that is discovered to have non-negligible impact

risk with less than about 10 years of warning time would need to be fragmented in order to elevate the threat. Also, given that the size of the asteroid is assumed to be between 100 and 500 m in diameter, civil defense is not a feasible option to deal with the asteroid threat and deflection is not a very promising option. Given that the time frame is too short and the asteroid is too large for a deflection mission to have enough of an effect on the orbit to guarantee a safe passage of the asteroid by the Earth, the best option for humanity to avoid getting hit by the whole asteroid would be to fragment the body and give the fragments time to disperse over the asteroid's orbital path. A successful asteroid fragmentation would mean that the Earth would at worst have to deal with a small fraction of the asteroid mass impacting the planet, a far better alternative than having the entire asteroid mass making landfall as a single solid piece.

4. Impact and keyhole passage risk assessment

This section provides a discussion of the methods employed to assess the possibility of an asteroid or asteroid fragment impacting the Earth or passing through a gravitational keyhole to impact the planet at a future date.

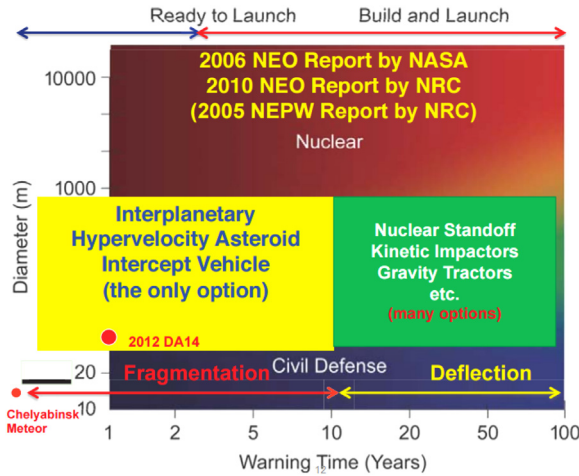


Fig. 4. A summary of mitigation strategies based on the warning time and the asteroid diameter size.

4.1. Impact risk assessment

One of the simplest ways, in theory not necessarily computationally, of estimating the impact probability between an asteroid and a planet is to simply construct a field of virtual asteroids about the reference trajectory of the asteroid, propagate them all through the anticipated encounter date, and calculate the impact probability by dividing the number of virtual asteroids that hit the planet, known as virtual impactors, by the total number of virtual asteroids used in the computation. A drawback of this method is that it can be computationally expensive, and the number of virtual asteroids that would need to be used needs to be at least equal to the inverse of the impact probability [16] – meaning that there needs to be some prior knowledge of the impact probability, which is the unknown quantity to be computed. Alternative methods of impact probability computation have been developed in the literature by using an impact probability model of the form

$$IP = \int \int \int_{V_{\oplus}} PDF(x, y, z) dx dy dz \quad (11)$$

It has been shown previously [19] that to simplify the calculation, the three-dimensional PDF can be simplified to one-dimension by converting the (x, y, z) position data to spherical coordinates (r, θ, ϕ) , and the triple integral would turn into a single integral over the radius of Earth,

$$IP = \int_0^{r_{\oplus}} PDF(r) dr = CDF(r_{\oplus}) - CDF(0) \quad (12)$$

where CDF denotes the cumulative density function resulting from the radial PDF. For this case, the entire domain is considered to be the Earth's B-plane, but the region of particular interest is the radial cross-section of the Earth – hence the integration limits of zero and r_{\oplus} . Based on the referenced formulation of the problem, the

CDF takes the form

$$IP = \frac{1}{2} \left[\operatorname{erf} \left(\frac{r_{\oplus} - \mu}{\sigma \sqrt{2}} \right) - \operatorname{erf} \left(\frac{0 - \mu}{\sigma \sqrt{2}} \right) \right] \quad (13)$$

where the difference between the CDF value at zero and at Earth's radius results in a difference in the error function, in terms of the mean (μ) and standard deviation (σ) of the virtual asteroid close-approach radii. So, the calculated value for the impact probability over the entire Earth can be found by narrowing the region of interest from the entire Earth B-plane to the cross-section of the Earth on it.

The formulation is incorrect in that analysis however, particularly Eq. (13). If the initial variations in (x, y, z) position are normally distributed about their own means and the associated standard deviations, then the resulting error function stemming from the radial PDF would be incorrect. The probability density function of the error function is a normal distribution, meaning that the radius values of the close-approach values would have to be normally distributed, which is not true given that (x, y, z) are normal and $r = \sqrt{x^2 + y^2 + z^2}$. The radial distribution would be Rayleigh or shifted Rayleigh, using two normally distributed, independent variables (x, y) , or even two planar orthogonal coordinates (e.g., (ξ, ζ)) [17]. The vector magnitude of the crossing points would be a Rayleigh distribution, assuming that the components are uncorrelated with equal variance and zero mean. The crossing data will not necessarily have equal variance or zero mean, so a distribution (some type of gamma distribution possibly) can be fit to the radial position data in order to find a better estimate of the impact probability. Having a larger pool of virtual asteroids used in the computation increases the computation time, but should yield a more accurate impact prediction.

4.2. Keyhole passage risk assessment

When looking for the possibility of a body passing through a keyhole on a planet's target B-plane, looking simply at the radial distribution of the close-approach data does not distinguish between data points that are in the correct region of the B-plane and those that have the component combinations that would result in the radial distance associated with a keyhole. Different methods exist to answer that question, such as long-term orbital simulations tracking the asteroids (or asteroid fragments) or analytic keyhole theory to find the regions in an encounter B-plane that would result in a resonant return with the planet. Each method has a cost associated with it – the long-term orbital simulations can take a large amount of computation time but are fairly high-fidelity, while the analytic theory takes a significantly smaller amount of computation time while providing lower-fidelity results.

The virtual fragments constructed through the orbital uncertainty of a single asteroid fragment propagated through the encounter B-plane occupy a fraction of the B-plane's area. The keyhole on the same encounter B-plane also occupies a fraction of the B-plane area, however, not necessarily the same or even overlapping areas of the B-plane. Based on the analytic keyhole theory discussed

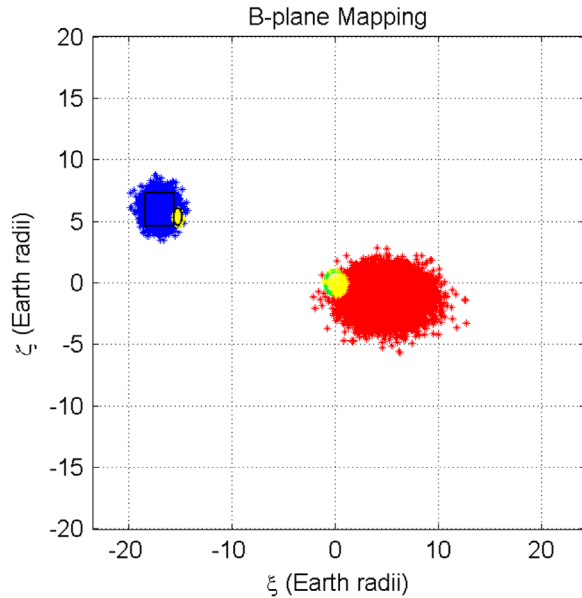


Fig. 5. Example composite encounter B-plane for successive encounters of an asteroid with Earth. The cluster of blue and yellow stars to the left indicate the B-plane crossing locations on the first encounter, and the cluster of red and yellow stars near the origin indicate the B-plane crossing locations on the second encounter. (For interpretation of the references to color in this figure caption, the reader is referred to the web version of this paper.)

previously, a body that passes through a gravitational keyhole on a target B-plane will in the future come to have an impact encounter with the planet on the next encounter, it is clear that there is a mapping between the keyhole region of one B-plane and the Earth cross-section on a second B-plane. Therefore, by simply counting the number of virtual asteroids that pass into the keyhole region, found from the analytic theory, an estimate can be formed of the impact probability of the asteroid on the second encounter B-plane, without having to simulate the orbits of those virtual asteroids through both encounters.

For example, assume that an asteroid has a virtual asteroid cloud, comprising 10,000 virtual asteroids, passing through the Earth's encounter B-plane such as that indicated by the blue and yellow stars (first encounter) and the red and yellow stars (second encounter) showing the position of the same virtual asteroid cloud on the next encounter B-plane, in Fig. 5. In this figure the Earth's cross-section is projected onto the composite B-plane and is depicted as a green circle with a radius of one centered about the origin. The yellow stars in each cloud indicate the virtual asteroids that pass within 1.1 Earth radii on the second encounter B-plane. It is worth mentioning that the crossing points on the first encounter B-plane were created such that the probability of an impact with the planet on the first pass is zero. Of the 10,000 virtual asteroids crossing locations on the second encounter B-plane, 66 fall within 1.1 Earth radii of Earth's center, making the impact probability for the encounter 0.66%. That would mean, that there is a 0.66% probability that the blue stars of the first encounter will fall within the black ellipse representing the keyhole region on the first encounter B-plane.

Looking at the data, the estimated impact probability of the virtual asteroid cloud after the first encounter with the Earth is estimated as

$$\hat{IP} = \frac{N_e}{N} \approx \frac{1}{N} \text{Binomial}(N, IP) \quad (14)$$

where \hat{IP} is the estimated impact probability value, N_e is the number of virtual asteroid crossing points that fall inside the ellipse (keyhole), N is the number of total virtual asteroids simulated, $\text{Binomial}()$ is a binomial distribution, and IP is the true impact probability (which is unknown). It is known that the mean impact probability value, based on this binomial formulation of the estimated impact probability, is simply the mean of all the estimated impact probability values

$$\mu = \text{mean}(\hat{IP}) = IP \quad (15)$$

where μ represents the mean impact probability value. It follows that the impact probability estimator, Eq. (14), is unbiased. It is also easy to show that the estimator has a standard deviation given by

$$\sigma = \text{std}(\hat{IP}) = \frac{1}{\sqrt{N}} \sqrt{IP(1-IP)} \quad (16)$$

where σ is the standard deviation.

The only problem here is that the true impact probability (IP) is unknown, if it was not then there would not be a need for any of this, but if an upper bound was placed on what the true value of the impact probability is, an assessment can be made as to how good the estimated impact probability based on the number of virtual asteroids simulated. Take the previous, fictitious example shown in Fig. 5 as an example. Suppose that we are almost guaranteed that $IP < 0.1$ ($< 10\%$), then the standard deviation, using 10^4 simulated virtual asteroids, is calculated to be 0.003. If it is assumed that the 0.66% value found earlier is the true impact probability value, then about two standard deviations to the left of the mean are zero, according to our distribution. So, under the established assumption that the impact probability is less than 10%, we cannot assume that \hat{IP} is normal, and may be some kind of Rayleigh based on the two normally distributed, independent variables example discussed previously. Let us assume that we know for a fact that the true impact probability is less than 2%. Rerunning the standard deviation calculation, using 10^4 simulated virtual asteroids, the standard deviation value is found to be 0.0014. Now, zero is nearly five standard deviations to the left of the mean, meaning that we could assume that \hat{IP} is normally distributed (based on invocation of the Central Limit Theorem). Depending on how conservative we are in regards to the upper bound of the true impact probability, an understanding can be gained as to how good the estimated impact probability value is in regards to the assumed distribution.

5. Analytic keyhole theory

Before getting into the mission design and potential fragmentation of the fictitious asteroid 2015 PDC, the

concepts of a target B-plane and a gravitational keyhole need to be specifically defined.

5.1. Target planes

A target plane is defined as a geocentric plane oriented to be normal to the asteroid's geocentric velocity vector. Observing the point of intersection of an asteroid trajectory with the target plane can lend significant insight into the nature of a future encounter. In general, there are two distinct planes and several coordinate systems that can be used in such a framework. The classical target plane is referred to as the B-plane, which has been used in astrodynamics since the 1960s. The B-plane is oriented normal to the incoming asymptote of the geocentric hyperbola, or normal to the unperturbed relative velocity \vec{V}_∞ . The plane's name is a reference to the so-called impact parameter b , the distance from the geocenter to the intercept of the asymptote on this plane, known as the minimum encounter distance along the unperturbed trajectory [16]. Fig. 6 depicts the relationship between the target B-plane and the trajectory plane of the asteroid. The system of coordinates that will be used for the analyses conducted in this paper (ξ, η, ζ) are described later, while those shown in the figure are just an example of a coordinate system that could be used.

5.2. Target plane coordinates

Generally it is convenient to place the origin of the B-plane's coordinate system at the geocenter, but the orientation of the coordinate axes on the plane is arbitrary. The coordinate system is fixed at times by aligning the axes in a way so that one of the nominal target plane

coordinates is zero, or by aligning one of the coordinate axes with either the projection of the Earth's polar axis or the projection of the Earth's heliocentric velocity.

One of the most important functions of the target plane is to determine whether a collision is possible, and if not, how deep the encounter will be. With the B-plane, we obtain the minimum distance of the unperturbed asteroid orbit at its closest approach point with the Earth – the impact parameter b . That single variable however does not tell whether the asteroid's perturbed trajectory will intersect the image of the Earth on the following encounter, but the information can be extracted by scaling the Earth radius R_\oplus according to the following relationship:

$$b_\oplus = R_\oplus \sqrt{1 + \frac{V_e^2}{V_\infty^2}} \quad (17)$$

where V_e is the Earth escape velocity

$$V_e = \sqrt{\frac{2GM_\oplus}{R_\oplus}} \quad (18)$$

With this formulation a given trajectory impacts the Earth if $b < b_\oplus$, and would not otherwise. Alternatively, the impact parameter could be scaled while leaving the image of the Earth on the B-plane unchanged. The two scalings are equivalent for a single orbit, but when computing the coordinates for different asteroids with different \vec{V}_∞ , the scaling is not uniform [18].

A convenient and common target plane coordinate system (ξ, η, ζ) is obtained by aligning the negative ζ -axis with the projection of the Earth's heliocentric velocity \vec{V}_\oplus , the positive η -axis with the geocentric velocity (normal to the B-plane), and the positive ξ -axis in such a way that the reference frame is positively oriented, expressed by the following

$$\vec{\eta} = \frac{\vec{V}_\infty}{|\vec{V}_\infty|} \quad (19)$$

$$\vec{\xi} = \frac{\vec{\eta} \times \vec{V}_\oplus}{|\vec{\eta} \times \vec{V}_\oplus|} \quad (20)$$

$$\vec{\zeta} = \vec{\xi} \times \vec{\eta} \quad (21)$$

where \vec{V}_∞ is the geocentric velocity vector of the asteroid, which is invariant under the body's encounter with the Earth. With this reference frame, it can be seen that $\vec{\xi}$ and $\vec{\zeta}$ are on the B-plane itself, where (ξ, ζ) are the target plane coordinates that indicate the cross track and along track miss distances, respectively. That way, ζ is the distance in which the asteroid is early or late for the minimum possible encounter distance. The early or late timing of the asteroid crossing the target plane ($\eta = 0$) is given by

$$\Delta t = \frac{\zeta}{V_\oplus \sin \theta} \quad (22)$$

where θ is the angle between \vec{V}_∞ and \vec{V}_\oplus . The ξ coordinate, on the B-plane, refers to the minimum distance achieved by altering the timing of the encounter between the asteroid and the Earth, known as the Minimum Orbital Intersection

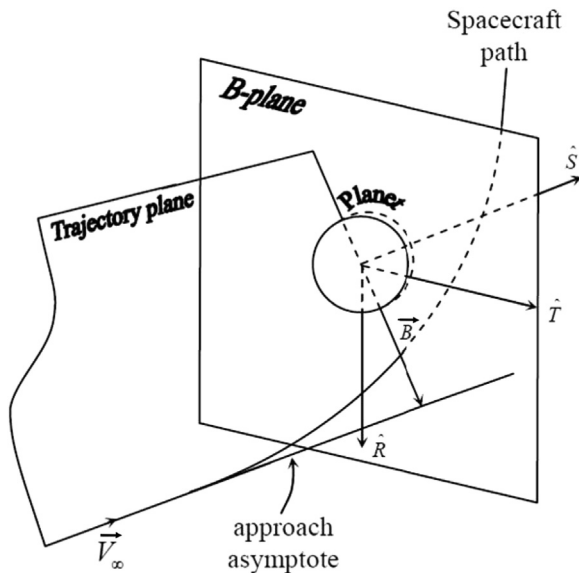


Fig. 6. Representation of the target B-plane of a planet with respect to the incoming approach of a body on the trajectory plane. The coordinate system used in this figure is the system used by Dr. George Born from the University of Colorado at Boulder in a class on Interplanetary Mission Design [16].

Distance (MOID). It is important to note that this particular interpretation of the coordinates of the B-plane is only valid in the linear approximation, and unusable for distant encounters beyond several lunar distances.

Such a formulation of the problem gives rise to thought that an asteroid can avoid impact if either the timing of the encounter is off or by being in an orbit that does not even intersect the Earth's orbit. Therefore, to have an impact occur the asteroid must have a small enough MOID and be on time for the encounter. So, an encounter can be well-defined given only the MOID and the Δt . The manner in which the encounters are characterized in this paper are according to the analytic theory developed by Valsecchi et al. [18].

5.3. Resonant returns and keyholes

A resonant return orbit is a consequence of an encounter with Earth, such that the asteroid is perturbed into an orbit of period $P' \approx k/h$ years, with h and k being integers. After h revolutions of the asteroid and k revolutions of the Earth, both bodies are in the same region of the first encounter, causing a second encounter between the asteroid and the Earth.

The analytic theory of resonant returns that has been developed by Valsecchi et al. [18] treats close encounters with an extension of Opik's theory, adding a Keplerian heliocentric propagation between the encounters. The heliocentric propagation establishes a link between the outcome of the first encounter and the initial conditions of the next one. During the Earth encounter, the motion of the asteroid is assumed to take place on one of the asymptotes of the encounter hyperbola. The asymptote is directed along the unperturbed geocentric encounter velocity \vec{V}_∞ , crosses the B-plane at a right angle, and the vector from the Earth to the intersection point is denoted by \vec{B} [16].

According to Opik's theory, the encounter of the asteroid with the Earth consists of the instantaneous transition, when the body reaches the B-plane, from the pre-encounter velocity vector \vec{V}_∞ to the post-encounter velocity vector \vec{V}'_∞ , such that $V'_\infty = V_\infty$. And, the angles θ' and ϕ' are simple functions of V_∞ , θ , ϕ , ξ , and ζ , where θ is the angle between \vec{V}_∞ and the Earth's heliocentric velocity \vec{V}_\oplus and ϕ is the angle between the plane containing \vec{V}_∞ and \vec{V}_\oplus and the plane containing \vec{V}_\oplus and the ecliptic pole. The deflection angle γ is the angle between \vec{V}_∞ and \vec{V}'_∞ , described by

$$\tan \frac{\gamma}{2} = \frac{q}{b} \quad (23)$$

where $q = GM_\oplus / V_\infty^2$. In addition, simple expressions relate (a, e, i) to (V_∞, θ, ϕ) , and (ω, Ω, ν) to (ξ, ζ, t_0) , where t_0 is the time at which the asteroid passes the node closer to the encounter [16,18].

A resonance orbit corresponds to certain values of a' and θ' that can be denoted by a'_0 and θ'_0 . If the post-encounter is constrained in such a way that the ratio of

periods between the Earth and the asteroid is k/h , then we have

$$a'_0 = \left(\frac{k}{h} \right)^{2/3} \quad (24)$$

$$\cos \theta'_0 = \frac{1 - V_\infty^2 - 1/a'_0}{2V_\infty} \quad (25)$$

$$\cos \theta'_0 = \cos \theta \frac{b^2 - q^2}{b^2 + q^2} + \sin \theta \frac{2q\xi}{b^2 + q^2} \quad (26)$$

Thus, for a given V_∞ , θ , and θ'_0 , we have

$$\cos \theta'_0 = \cos \theta \cos \gamma + \sin \theta \sin \gamma \cos \psi \quad (27)$$

in the pre-keyhole B-plane, which gives the locus of points leading to a given resonant return.

6. Mission Designs for Asteroid 2015 PDC

The fictional asteroid 2015 PDC was detected on April 13, 2015 and is believed/known to be on an Earth-impacting trajectory, with a predicted impact on September 3, 2022. That means that there is about a seven-year time window for reconnaissance or deflection/disruption mission attempts. Although the asteroid is only estimated to have a 0.2% impact probability shortly after its discovery, a rendezvous mission to the target body can be considered in order to gain more information about the asteroid's orbit and physical parameters. Once a rendezvous mission has launched and had some time near the target, a disruption mission to the hazardous body can be launched to try and mitigate the threat to Earth. In order to study the feasibility of a mission to leave Earth and arrive at asteroid 2015 PDC, porkchop plots are constructed. A porkchop plot is a contour plot that shows the amount of launch energy or mission ΔV needed to leave one particular orbit and enter into another, based on the departure date and the transfer time. The mission durations are expressed in days, while the departure dates are shown using the Julian date. The Julian date is essentially the day of year number that refers to a specific date in the Gregorian calendar. The porkchop plots departure dates all span the same timespan, from the date of discovery of the asteroid (April 13, 2015) to the expected impact date (September 3, 2022).

6.1. Rendezvous mission designs

For a rendezvous mission, one of the most important parameters to consider, beyond the ability to place the spacecraft into the appropriate trajectory to meet the target, is the speed at which the spacecraft approaches the target. If that speed is too large, the spacecraft would require a large amount of propellant in order to make up the speed difference. Therefore, one of the quantities to be minimized through the mission optimization process is the total mission ΔV . Fig. 7 shows the resulting rendezvous mission ΔV porkchop plot for asteroid 2015 PDC.

Looking at the porkchop plot, it is easy to see that there are only a handful of regions where potentially feasible

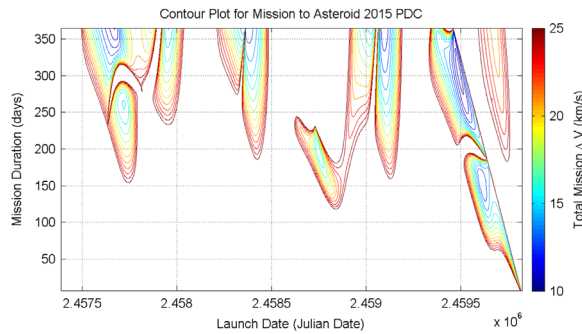


Fig. 7. Porkchop plot of total mission ΔV for a rendezvous mission to asteroid 2015 PDC before its potential Earth impact in 2022.

rendezvous missions could exist to this asteroid body. Most of the potentially mission feasible regions lie at the top of the porkchop plot, where the mission durations are highest. There is one region however that could have feasible missions around 150 days in duration, but the launch date is about a year prior to the expected impact date. Such a late launch date for a rendezvous mission does not really allow for the potential of several disruption mission attempts, in the case that they fail or do not have the desired effect. In order to allow for a larger window in which disruption missions can be conducted, the time between target acquisition and the expected impact date, within the AMiDST program, will have a lower bound limit of 1000 days (about 3 years).

Total mission ΔV and acquisition time are only two of the important mission parameters needed to evaluate mission logistics, the mission V_∞ is also needed in order to assess the relative ease with which the launch vehicle can set the spacecraft in its interplanetary orbit. A lower mission V_∞ would indicate that the interplanetary orbit would be easy to enter into, after leaving the Earth's sphere of influence. On the other hand, a higher mission V_∞ would be either because the energy of the hyperbolic orbit needed to enter into the required interplanetary trajectory is very large or the interplanetary trajectory is out of the ecliptic plane. Fig. 8 shows the rendezvous mission V_∞ porkchop plot for asteroid 2015 PDC. Observing the porkchop plot, it can be seen that the low mission V_∞ values exist in the same regions as the low mission ΔV values, and in a couple other regions as well. In those regions where the V_∞ values are low and the ΔV values are not, it would imply that the relative arrival velocity between the spacecraft and the target body is the larger contributor to the overall mission ΔV . Despite the requirement and limitations placed on the value of the mission V_∞ , in regards to the optimal rendezvous mission, the limiting factor in this particular mission design will be the total mission ΔV and the relative arrival speed.

In order to find the optimal rendezvous mission for a spacecraft mission to asteroid 2015 PDC, the following mission parameters were chosen as a part of the optimization process: launch date, total mission ΔV , mission C3, target acquisition time, mission duration, and relative arrival speed. The resulting mission trajectory is shown in Fig. 9. The green line indicates the track that Earth takes during the time that it takes the spacecraft (blue line) to

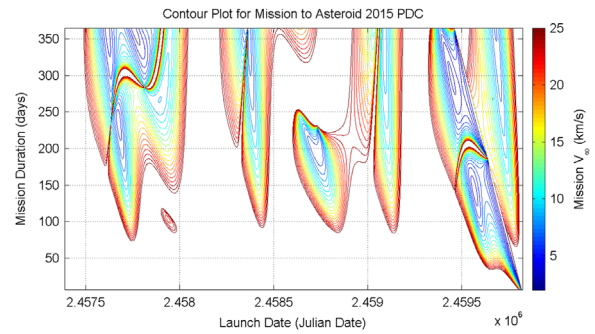


Fig. 8. Porkchop plot of mission V_∞ for a rendezvous mission to asteroid 2015 PDC before its potential Earth impact in 2022.

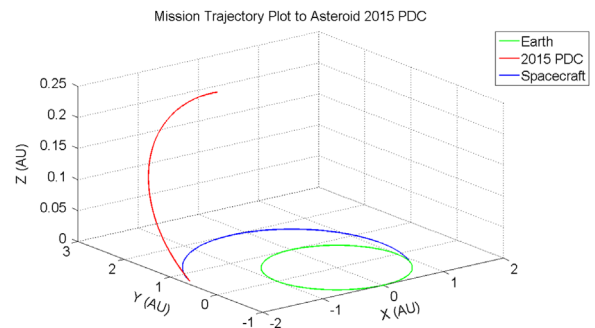


Fig. 9. Trajectory plot for the optimal rendezvous mission to asteroid 2015 PDC between its discovery date and the expected impact date between asteroid 2015 PDC and the Earth. (For interpretation of the references to color in the text, the reader is referred to the web version of this paper.)

arrive at asteroid 2015 PDC (red line). Within the time that it would take the Earth to complete one revolution, the spacecraft launched on September 5, 2018 would arrive at asteroid 2015 PDC and begin its reconnaissance mission. The launch window surrounding this optimal mission is fairly small, about four days in length. Despite the limited length of the launch window, the remaining of the top ten missions occur within that same launch window but with varying length of mission durations. From that optimal launch window, there would be around 1094 days between the spacecraft's encounter of the asteroid body and the expected impact date for the spacecraft to observe the physical parameters of the body and track the asteroid's orbit track around the Sun.

Based on the shape of the spacecraft trajectory for the optimal rendezvous mission depicted in Fig. 9, the spacecraft has to be launched from Earth's sphere of influence on a fairly high energy hyperbolic orbit ($C3 \approx 26.5 \text{ km}^2/\text{s}^2$) because while the interplanetary orbit stays near the Earth's ecliptic plane, the trajectory reaches beyond Mars orbit and encounters the asteroid body nearly 2 AU from the Sun (almost 3 AU from Earth). The total mission ΔV is about 12.38 km/s, about 8 km/s of which are needed by the spacecraft upon arrival to match the asteroid's speed. Based on the resulting optimal rendezvous mission parameter values, the necessary ΔV that the spacecraft needs to match the asteroid's speed is relatively large – meaning that the spacecraft needs to be large enough to hold the

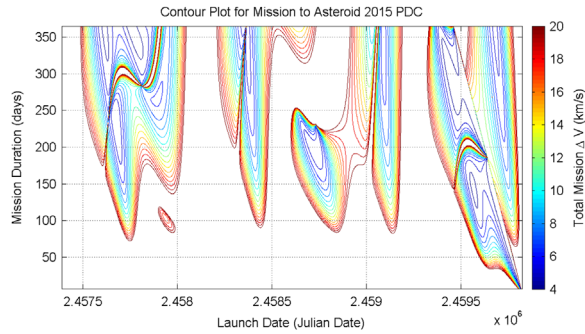


Fig. 10. Porkchop plot of total mission ΔV for an intercept mission to asteroid 2015 PDC before its potential Earth impact in 2022.

necessary fuel needed to make that change in speed. In fact, about 85% of the total spacecraft mass would need to be fuel in order to successfully achieve such a large velocity change. So, if the largest version of the HAIV spacecraft is chosen to carry out this mission (mass of 5720 kg), then only about 950 kg of the spacecraft mass would be available to be used for the payload, structure, and instrument suites.

6.2. Disruption mission designs

The optimization process would be conducted for disruption missions in much the same way as for rendezvous missions, but would ignore the relative arrival speed of the spacecraft to the target asteroid. Before looking at different mission design types ((1) long-duration, long-dispersion, (2) long-duration, short-dispersion, (3) short-duration, long-dispersion, and (4) short-duration, short-dispersion), the total mission ΔV (Fig. 10) and V_∞ (Fig. 11) porkchop plots can be analyzed to understand how accessible asteroid 2015 PDC is from Earth between 2015 and 2022 for a disruption mission. Examining Fig. 10, it can be seen that short-duration missions (less than 100 days) would be very difficult to be realized for a spacecraft, outside a few months before the expected impact date. When looking at mission durations of more than 100 days, it appears that there are periodic regions of the porkchop plot where an intercept mission can be launched to asteroid 2015 PDC. The V_∞ porkchop plot in Fig. 11 validates the notion that short-duration missions would be hard to come by before the few months prior to the expected impact. Observing the remaining portion of Fig. 11, it can be seen that the accessible regions of the porkchop plot are smaller than what they appeared to be in ΔV porkchop plot. Based on the V_∞ porkchop plot, the easiest times to launch a mission would be soon after its discovery (around the 2015/2016 time frame) and within a year of the anticipated impact date. Due to the lateness of the rendezvous mission's departure date and our research focus on short-warning times, the mission types that will be looked at will be long-duration, short-dispersion and short-duration, short-dispersion mission designs. The rendezvous mission arrives at the target body nearly three years prior to the expected impact date, but to give time for the spacecraft to gather enough information about the orbit and the physical characteristics of the

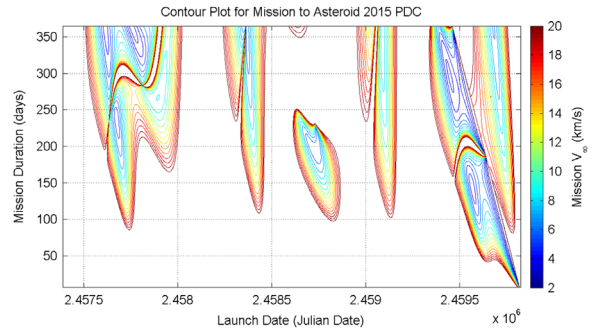


Fig. 11. Porkchop plot of mission V_∞ for an intercept mission to asteroid 2015 PDC before its potential Earth impact in 2022.

asteroid, the mission designs discussed here will focus on dispersion times between seven and 90 days in length – true last minute disruption missions.

6.2.1. Short-duration, long-dispersion mission

As already stated, the ability to conduct a feasible short-duration, long-dispersion mission is not practical. However, this mission type is the most desirable disruption mission type given its tendency to maximize the amount of time from launch to the anticipated impact date. For the case of asteroid 2015 PDC, the optimal short-duration, long-dispersion mission results are discussed here briefly to show its impracticality.

The required mission ΔV and C3 orbit for a short-duration, long-dispersion mission scenario would be too large for any launch vehicle currently in operation to place even a small spacecraft into the necessary orbit to intercept the target body. None of the top 10 optimal missions are feasible: the mission ΔV is nearly 14 km/s from LEO and the required orbit C3 is about $350 \text{ km}^2/\text{s}^2$. The trajectory depicted in Fig. 12 gives justification for the highly energetic orbit required by the spacecraft to leave Earth and meet 2015 PDC. The optimization process tried to push the mission duration as high as possible, in an attempt to reduce the required ΔV and C3, but the restriction of a maximum mission duration of 90 days did not allow for more feasible missions to be considered in this analysis. The date at which this short-duration, long-dispersion mission would launch would be in the middle of a launch window centered on December 18, 2016, a little more than a year and a half after discovery of asteroid 2015 PDC. To compound the difficulty of this mission design, if there was some way of getting the spacecraft into the required interplanetary orbit, there would be the added difficulty of the hypervelocity encounter between the spacecraft and asteroid. In this case the relative arrival speed between the two bodies comes to be about 35 km/s, much faster than any relative arrival speed found in other mission designs conducted. It is possible that a more feasible optimal mission design could be obtained with an alternate definition of short-duration, but for the sake of consistency between this example asteroid, and the other asteroids studied [4], the definition is unaltered.

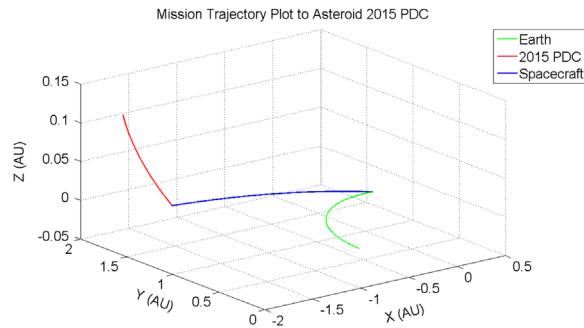


Fig. 12. Trajectory plot for a short-duration, long-dispersion intercept mission to asteroid 2015 PDC.

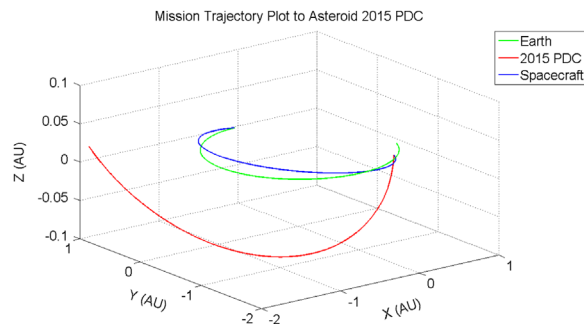


Fig. 13. Trajectory plot for a long-duration, short-dispersion intercept mission to asteroid 2015 PDC.

6.2.2. Long-duration, short-dispersion mission

Trying to keep the mission duration as long as possible should reduce the necessary amount of mission ΔV needed to get into the required orbit. The best long-duration, short-dispersion mission results in a total ΔV requirement of 3.273 km/s, most of which would be provided by the launch vehicle leaving from LEO, and a mission C3 of about $1 \text{ km}^2/\text{s}^2$. And with a spacecraft mass of about 2500 kg, this mission is easily feasible for most any launch vehicle to accomplish. The top mission trajectory to asteroid 2015 PDC does not deviate from the ecliptic much and does not need to go far outside the Earth's vicinity, which explains the small C3 value and is made evident in Fig. 13. The cost function algorithm was allowed to evaluate missions with durations between 200 and 365 days, where the dispersion time after the spacecraft encounters the target asteroid must fall between 7 and 90 days. The top resulting mission design had a mission duration of 245 days and a dispersion time of 7 days. In fact, this mission was in the middle of a 10 day launch window of optimal missions, where all optimal missions had dispersion times of 7 days, despite the allowance for more time, and the variation in launch date resulted in a corresponding change to the mission duration. The length of the mission duration and launch date correspond to the short dispersion time, and with an expected spacecraft encounter one week prior to Earth impact, the relative arrival speed between the spacecraft and the asteroid is understandably over 10 km/s, meaning that the guidance algorithms would need to be

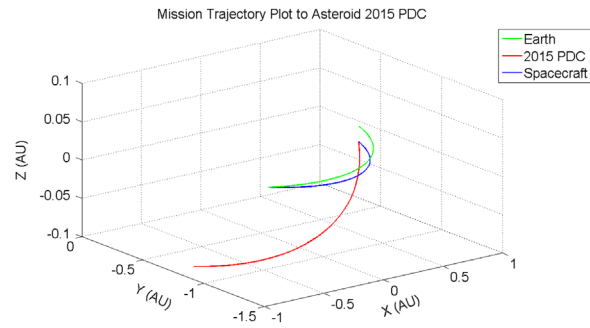


Fig. 14. Trajectory plot for a short-duration, short-dispersion intercept mission to asteroid 2015 PDC.

fast-responding and highly precise because there is no room for failure.

6.2.3. Short-duration, short-dispersion mission

Assuming that it is too late for all other options, or even worse they have all failed, to diminish the threat posed by asteroid 2015 PDC, a short-duration, short-dispersion mission design is constructed to deal with the imminent threat from the target asteroid. A short mission duration and short dispersion time implies that the asteroid has now entered the terminal phase of its orbit with respect to the Earth. Thus, with such a late launch window, the task of reaching the asteroid from Earth should be simpler to accomplish. The additional constraint of a short mission duration means that the mission duration has the same time restraint as the dispersion time (7–90 days). The optimal mission trajectory, depicted in Fig. 14, shows the simplicity of the orbit needed by the spacecraft to leave Earth and intercept the asteroid. The results from cost function evaluations show that the longer the mission duration and the shorter the dispersion time for the desired intercept trajectory would produce a more manageable design. Low total mission ΔV and C3 values allow for larger spacecraft and/or smaller launch vehicles to be used, but the hypervelocity relative arrival speed ($\approx 12 \text{ km/s}$) between the spacecraft and the asteroid mandates the use of a spacecraft similar to the HAIV for any attempted fragmentation mission.

Despite the ease of these types of mission designs, late launch date and short-dispersion time, it should be noted that they should be considered as a last resort when all other attempts have failed, and not considered only when there are no other options able to be taken.

7. Fragmentation of Asteroid 2015 PDC

Because our research is focused on short warning times, the time from the disruption event to the asteroid fragments encountering the planet is set to be one year. Assuming that the fragment states are normally distributed about the nominal asteroid trajectory's states, before the radial perturbation is applied to each fragment, the fragments are propagated over that year time span through to their individual encounters with the Earth. The resulting crossing points of the 10,001 constructed virtual asteroid fragments on the encounter B-plane are shown in Fig. 15.

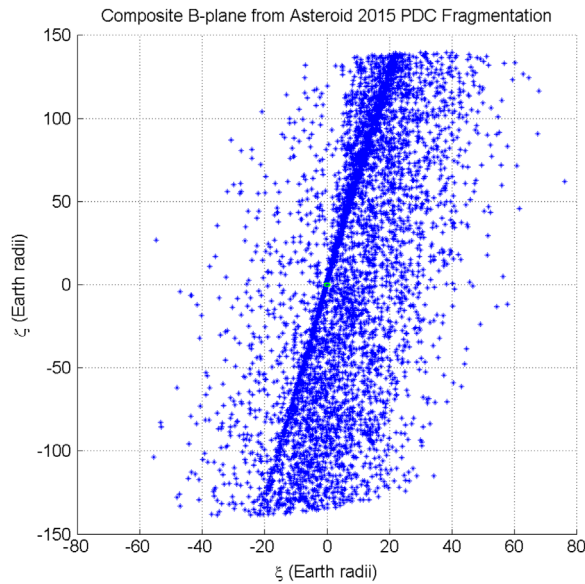


Fig. 15. Composite encounter B-plane showing the crossing locations of asteroid 2015 PDC's fragments.

It can be seen from the composite B-plane that the asteroid fragments are spread across a wide portion of the map. For reference, a small circular cross-section of the Earth can be seen centered at the origin.

Of the numerous simulated fragments of asteroid 2015 PDC, a fragment is selected that crosses the B-plane fairly close to the Earth (about 9 Earth radii from the center of the planet). Using state standard deviations of 10 m and 1 m/s, normally distributed about the nominal asteroid fragment states, a field of 10,000 virtual fragments is created and propagated through the encounter B-plane, in addition to the nominal asteroid fragment's trajectory. Fig. 16 shows the crossing locations of the virtual fragment field on the encounter B-plane. It can be seen that the 2015 PDC fragment cloud encompasses the Earth. In fact, about 2.9% of the 10,001 simulated virtual fragments pass within 1.1 Earth radii of the center of the planet. A histogram of the radial distances of the fragment cloud crossing positions is shown in Fig. 17. The radial position histogram shows a skewed distribution, with a large portion of the data being between 0 and about 12 Earth radii. Fitting a gamma distribution to the radial position data, the calculated probability that the asteroid fragment would fall within 1.1 Earth radii is approximately 2.4%. The B-plane component distributions for the 2015 PDC asteroid fragment appear to be nearly normal. The histograms in Fig. 18 show the distributions of the fragment cloud's B-plane components. Looking at the ξ -component, the distribution appears to be pretty normal, with a mean a bit larger than one Earth radius. The ζ -component however appears to be comprised of two different normal distributions (one for the left portion of the distribution and one for the right portion).

Based on the 10,001 virtual asteroids simulated from a single asteroid fragment from the asteroid fragmentation event that had occurred a year prior to the encounter, the estimated impact probability of that particular asteroid

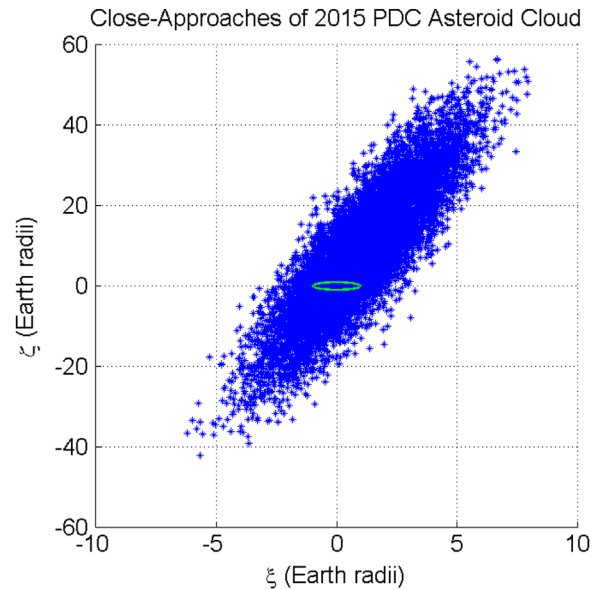


Fig. 16. Asteroid 2015 PDC fragment cloud crossing locations on close-encounter B-plane.

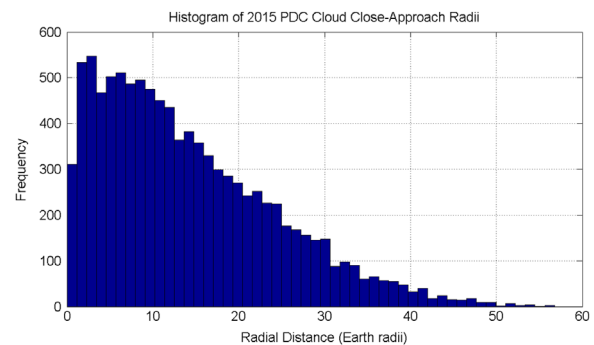


Fig. 17. Histogram of asteroid 2015 PDC's fragment cloud radial crossing locations.

fragment was found to be about 2.9%. Fig. 16 shows that the asteroid fragment cloud encompasses the cross-section of the Earth on the target B-plane, meaning that there the odds of the fragment impact the planet should not be ignored. In fact, using the results of this fragment cloud simulation where the estimated impact probability is 2.9% and the number of simulated virtual fragments is 10,001, the standard deviation of the estimator of the impact probability, assuming that the upper bound of the impact probability is assumed to be 5%, is about 0.0022. The zero of the impact probability distribution is over 13 standard deviations to the left of the assumed mean of 2.9%. Thus, it can be assumed that the impact probability estimator of this fragment is normal. The fact that the impact probability distribution can be assumed to be normal means that 10,000 virtual asteroid fragments is sufficiently large enough to get an accurate impact probability estimate of this asteroid fragment.

Switching from the future risk posed by the asteroid fragment to the Earth, Fig. 19 can be used to better understand the future risk imposed by the chosen

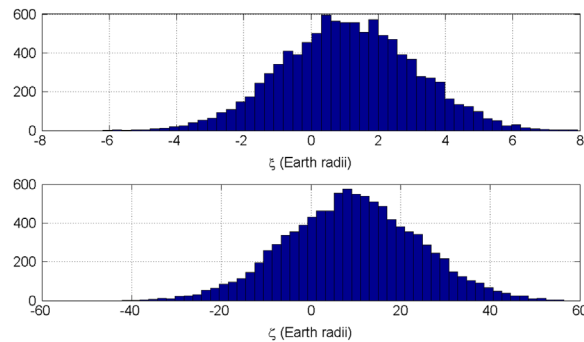


Fig. 18. Top: histogram of asteroid 2015 PDC's fragment cloud ξ components. Bottom: histogram of asteroid 2015 PDC's fragment cloud ζ components.

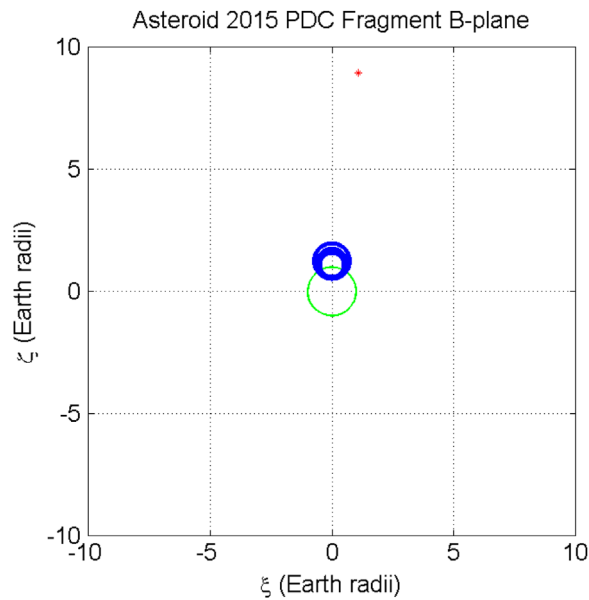


Fig. 19. Depiction of asteroid 2015 PDC's fragment resonance circles. The black vertical lines depict the corridor where the fragment's crossing location on the next encounter B-plane. The red star depicts the fragment's crossing location on the current encounter B-plane. (For interpretation of the references to color in this figure caption, the reader is referred to the web version of this paper.)

fragment. The plot shows three potential resonances that the asteroid fragment could fall into given its encounter with the Earth and the crossing location of the fragment's nominal trajectory, with respect to the cross-section of the Earth on the B-plane. However, this fragment's post-encounter trajectory does not fall into one of those resonance orbits. The calculated, expected crossing position of the asteroid fragment on the next encounter B-plane is at a ξ -value of about 120 Earth radii from the center of the Earth, nowhere near the small resonance circles. And according to analytic keyhole theory, the resonances represented by the blue resonance circles have no keyholes on the depicted 2022 B-plane, due to there being no intersections between the resonance circles and the expected ξ -value line on the future encounter. Just because this fragment does not present a risk to the Earth in the

near future, does not mean that the threat from this fragment is non-existent. There could be potential dangers to the Earth that go beyond the 10 year future that was looked at in this analysis. A different methodology must be used to adequately evaluate those future potential risks because of the length of time between the encounters and the perturbations that could sufficiently effect the orbit.

Looking back at Fig. 15, it seems that the Earth is sitting in a region of the B-plane map where there is a non-negligible chance of it getting hit by more than one asteroid fragment, given the modeled fragmentation event. If it is assumed that the fragmentation only produces the 10,001 asteroid fragments simulated in this example, only about 5200 of the 10,001 virtual asteroid fragments ended up having an immediate encounter with Earth, and only 15 of those passed with 1.1 Earth radii of the planet center. What that means is that given this type fragmentation event, with a year timespan for the asteroid fragments to disperse from the original asteroid's impact trajectory, the Earth would only be impacted with about 0.15% of the total asteroid mass, rather than the full asteroid mass if nothing were done to deflect/disrupt the target body. And, if the assumption is made that the mass of the asteroid is evenly distributed among the simulated asteroid fragments, the 15 impacting virtual asteroid fragments would only cause localized damage to the parts of the Earth they impact (if they make landfall), rather than the potential regional or global damage that could be caused by the full asteroid impacting the planet.

8. Conclusions

The threat of a fictional asteroid 2015 PDC, which is discovered about seven years prior to its expected impact date, has been discussed. The process of analyzing the impact risk of this asteroid and designing rendezvous and disruption missions has also been discussed, with an emphasis on the current and future risk posed. Given nothing but the initial asteroid state at a given epoch, an asteroid cloud was constructed using assumed orbital uncertainties based on those of similar near-Earth asteroids. Not surprisingly, as the orbital uncertainty decreased, the impact risk grew. After analyzing the asteroid fragment cloud, a representative fragment was selected to be analyzed in terms of its potential resonance orbits, keyhole existence on the encounter B-plane, and the likelihood of passing through those keyholes. The selected asteroid fragment has three very small possible resonance circles it could fall in, but the encounters on those future B-planes occur more than 100 Earth radii away from the Earth, meaning that there is no resonance or keyhole passage potential. The possibility of that fragment impacting the Earth however is non-negligible. Overall, asteroid 2015 PDC is regularly accessible from Earth for disruption missions, difficult to rendezvous with due to the shape and orientation of the orbit, has a fairly high impact risk if unabated, and if fragmented a year prior to its expected impact, the risk to Earth is less due to the number of fragments that would come near the Earth and the amount of mass that would encounter the planet.

References

- [1] (<http://neo.jpl.nasa.gov/pdc15/>).
- [2] A. Pitz, B. Kaplinger, G. Vardaxis, T. Winkler, B. Wie, Conceptual design of a hypervelocity asteroid intercept vehicle (HAIV) and its flight validation mission, *Acta Astronaut.* 94 (2014) 42–56.
- [3] B. Barbee, B. Wie, S. Mark, K. Getzandanner, Conceptual design of a flight demonstration mission for a hypervelocity asteroid intercept vehicle, *Acta Astronaut.* 106 (2015) 139–159.
- [4] G. Vardaxis, B. Wie, Near-earth object intercept trajectory design for planetary defense, *Acta Astronaut.* 101 (August–September) (2014) 1–15.
- [5] National Research Council, Effects of Nuclear Earth-Penetrators and Other Weapons, The National Academies Press, 2005.
- [6] B. Wie, B. Barbee, An Innovative Solution to NASA's NEO Impact Threat Mitigation Grand Challenge and Flight Validation Mission Architecture Development, Final Report of a NASA Innovative Advanced Concepts Phase 2 Study, December 2014.
- [7] NASA JSC Cost Estimating and Models, Advanced Missions Cost Model, 2007.
- [8] S. Wagner, B. Wie, B. Barbee, Target selection for a hypervelocity asteroid intercept vehicle flight validation mission, *Acta Astronaut.* 107 (2015) 247–261.
- [9] P.W. Chodas, D. Yeomans, Orbit Determination and Estimation of Impact Probability for Near Earth Objects, AAS 09-002, AAS/AIAA Space Flight Mechanics Meeting, 2009.
- [10] AGI Force and Environment Models, Solar Radiation Force, 2015.
- [11] D.K. Yeomans, P.W. Chodas, G. Sitarski, S. Szutowicz, M. Krolukowska, Cometary orbit determination and nongravitational forces, In: *Comets II*, The Lunar and Planetary Institute, 2004, pp. 137–152.
- [12] M.A. Sharaf, H.H. Selim, Final state predictions for J2 gravity perturbed motion of the earth's artificial satellites using bispherical coordinates, *NRIAG J. Astron. Geophys.* 2 (2013) 134–138.
- [13] B. Wie, et al., An Innovative Solution to NASAs NEO Impact Threat Mitigation Grand Challenge and Flight Validation Mission Architecture Development, NIAC Phase II Final Report, NASA Innovative Advanced Concepts Phase II Study, September 2012–September 2014.
- [16] A. Milani, S.R. Chesley, P.W. Chodas, G. Valsecchi, Asteroid close approaches: analysis and potential impact detection, In: *Asteroids III*, The Lunar and Planetary Institute, 2002, pp. 55–69.
- [17] H. Kobayashi, B.L. Mark, W. Turin, *Probability, Random Processes, and Statistical Analysis*, Cambridge University Press, 2012.
- [18] G.B. Valsecchi, A. Milani, P.W. Chodas, S.R. Chesley, Resonant returns to close approaches: analytic theory, *Astron. Astrophys.* (2001).
- [19] A. Pitz, C. Teubert, B. Wie, Earth-impact probability computation of disrupted asteroid fragments using GMAT/STK/CODES, in: AAS 11-408, AAS/AIAA Astrodynamics Specialist Conference, Girdwood, AK, August 1–4, 2011.

Further reading

- [14] A. Carusi, G.B. Valsecchi, R. Greenberg, Planetary close encounters: geometry of approach and post-encounter orbital parameters, *Celest. Mech. Dyn. Astron.* 49 (1990) 111–131.
- [20] G. Vardaxis, B. Wie, Impact risk assessment for a fragmented asteroid in Earth resonant orbits, in: AIAA-2014-4300, AIAA/AAS Astrodynamics Specialist Conference, San Diego, CA, August 4–7, 2014.
- [21] R. Battin, Solving Lambert's problem, In: *An Introduction to the Mathematics and Methods of Astrodynamics*, Revised Edition, AIAA Education Series, 1801 Alexander Bell Drive, Reston, VA, 1999 (Chapter 7).
- [22] G.H. Born, Design of the Approach Trajectory: B-plane Targeting, University of Colorado Boulder: ASEN 5519-Interplanetary Mission Design, 2005.
- [23] Near-Earth Object Survey and Deflection Study Report, NASA, 2006.
- [24] Defending Planet Earth: Near-Earth Object Surveys and Hazard Mitigation Strategies, Report No. 0-309-14968-1, National Research Council, National Academy of Sciences, 2010.